CHEMISTRY OF MATERIALS

pubs.acs.org/cm

Article

From CdSe Nanoplatelets to Quantum Rings by Thermochemical Edge Reconfiguration

Bastiaan B. V. Salzmann, Jara F. Vliem, D. Nicolette Maaskant, L. Christiaan Post, Chen Li, Sara Bals, and Daniel Vanmaekelbergh*

Cite This: *Chem. Mater.* 2021, 33, 6853–6859

Read Online

ACCESS | Metrics & More | Article Recommendations | Supporting Information

ABSTRACT: The variation in the shape of colloidal semiconductor nanocrystals (NCs) remains intriguing. This interest goes beyond crystallography as the shape of the NC determines its energy levels and optoelectronic properties. While thermodynamic arguments point to a few or just a single shape(s), terminated by the most stable crystal facets, a remarkable variation in NC shape has been reported for many different compounds. For instance, for the well-studied case of CdSe, close-to-spherical quantum dots, rods, two-dimensional nanoplatelets, and quantum rings have been reported. Here, we report how two-dimensional CdSe nanoplatelets reshape into quantum rings. We monitor the reshaping in real time by combining atomically resolved structural characterization with optical absorption and photoluminescence spectroscopy. We observe that CdSe units leave the vertical sides of the edges and recrystallize on the top and bottom edges of the nanoplatelets, resulting in a thickening of the rims. The formation of a central hole, rendering the shape into a ring, only occurs at a more elevated temperature.

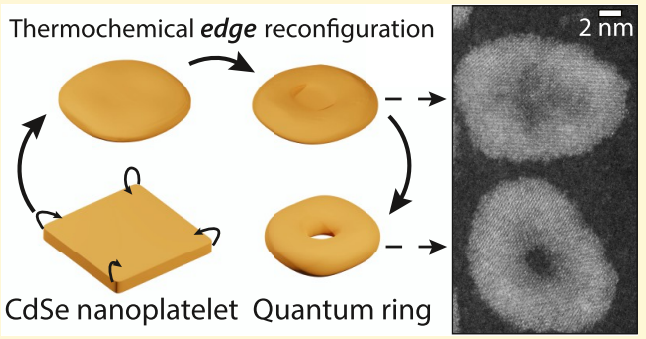

INTRODUCTION

The development of semiconductor nanocrystals (NCs) that show quantum confinement in one, two, or three dimensions, realizing bright emission and size- and shape-tailorable optical properties, has taken an enormous flight in the last three decades. For instance, a diversity of wet-chemical colloidal synthesis methods resulted in CdSe NCs with a wide variety in shape and size, ranging from sphere-like but facetted zero-dimensional (0D) quantum dots[1] to one-dimensional (1D) quantum rods[2] and two-dimensional (2D) nanoplatelets (NPLs).[3] We remark here that these shapes all belong to the genus = 0 class. Reports in the literature on the synthesis of colloidal quantum rings, i.e., with a genus of 1 topology, recently emerged.[4−10]

Ring-type CdSe NCs have been reported by Fedin et al.,[10] followed by more recent publications by others.[8,9] It was reported that the CdSe quantum rings have an in-plane linear distribution of transition dipole moments due to broken rotational symmetries[8] and exhibit exciton dynamics distinct from those in NPLs.[9] Moreover, the different topology in quantum rings can result in geometry-specific optoelectronic properties. Theoretical studies point to an excitonic Aharonov−Bohm effect, featuring a crossing of the exciton energy levels with increasing magnetic flux through the ring. Previous experimental work on solid-state quantum rings (type-I InAs/GaAs[11] and type-II (Zn,Mn)Te/ZnSe[12]) displayed a genuine quantum manifestation of the Aharonov−Bohm effect, which is observable as an oscillating intensity of the excitonic emission with increasing magnetic field. The oscillating intensity is caused by the difference in phase of the electron and hole wave functions in the ring, which varies periodically with the magnetic field. A zero phase difference corresponds to a maximum emission intensity.

Here, we report on a detailed investigation of the conversion of CdSe NPLs into quantum rings,[10] urged by the increasing interest in colloidal semiconductor quantum materials for optoelectronics and possibly for (quantum) information processing.[13] Our results show that the temperature during the thermal treatment of the NPLs with elemental selenium has a strong effect on the shape of the final quantum rings and that "intermediate shapes" (still of genus = 0 topological class) can be prepared with a remaining membrane of the same thickness as that of an original NPL. These findings challenge the formation mechanism put forward by Fedin et al., which

Received: May 11, 2021
Revised: August 11, 2021
Published: August 24, 2021

Downloaded via UTRECHT UNIV on December 2, 2021 at 08:50:14 (UTC).
See https://pubs.acs.org/sharingguidelines for options on how to legitimately share published articles.

ACS Publications

© 2021 The Authors. Published by American Chemical Society

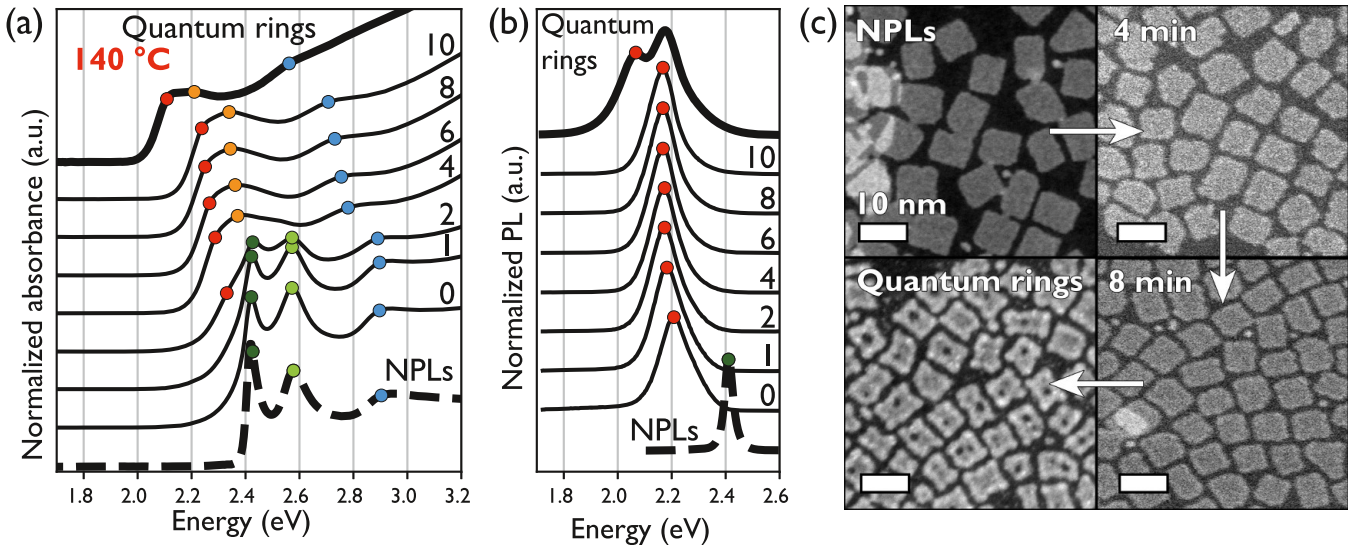

Figure 1. Monitoring the transformation of CdSe NPLs into quantum rings at 140 °C on aliquots in real time with optical spectroscopy and HAADF-STEM. (a) Absorption and (b) photoluminescence spectra of the dispersion of NPLs, aliquots taken after the mixture reached 140 °C (0 min), and after 1, 2, 4, 6, 8, and 10 min of reaction at 140 °C. For clarity, the evolving spectral features have been marked with colored circles (see the text and Figure S4). The continuous thick lines present the results for the sample that has been annealed at 220 °C following 10 min of reaction. (c) HAADF-STEM images of the original CdSe NPLs, NCs in the aliquots extracted at given times from the reaction at 140 °C, and the final quantum rings obtained after annealing at 220 °C following 10 min of reaction. All scale bars are 10 nm.

states that the top and bottom surfaces of the NPLs are etched by elemental selenium.

We investigated the formation of quantum rings in real time by extracting aliquots from the reaction mixture during the conversion at either 140 or 155 °C. We relate the structure of the intermediate NCs and finally formed quantum rings, obtained from high-angle annular dark-field scanning transmission electron microscopy (HAADF-STEM), to the optical absorption and photoluminescence spectra. Furthermore, we provide evidence for an atomic reconfiguration mechanism starting from the side edges and corners of the platelets, resulting in thicker rims on each platelet while leaving the central area of the platelets intact. One (or more) holes in the center of the NCs are only formed in the final annealing step at 220 °C, resulting in a genuine ring (genus = 1 class).

Additionally, we performed "muffin-tin" calculations considering the exciton as a composed but single particle and solving the Schrödinger equation for a realistic three-dimensional model of a CdSe NPL and quantum ring, as obtained from HAADF-STEM. The results were transformed to an energy level scheme for the confined excitons by considering the heavy-hole and light-hole excitons as composed "single particles" with a center-of-mass motion characterized by their effective reduced masses. Our calculations provide an energy gap between the heavy-hole and light-hole excitons in NPLs in reasonable agreement with the absorption spectrum and link this convincingly to the reduced separation observed in the CdSe rings due to weaker confinement. Reduced confinement also explains the strong red shift of the two absorption peaks and the red shift in the photoluminescence peak for the quantum rings compared to the original CdSe NPLs.

EXPERIMENTAL SECTION

Chemicals. 1-Butanol (BuOH, anhydrous, 99.8%), cadmium acetate ($Cd(OAc)_2$, 99.995%), cadmium acetate dihydrate ($Cd(OAc)_2{\cdot}2H_2O$, ≥98.0%), cadmium nitrate tetrahydrate ($Cd(NO_3)_2{\cdot}4H_2O$, 98%), methanol (MeOH, anhydrous, 99.8%), 1-octadecene (ODE, technical grade 90%), oleic acid (OA, technical grade 90%), oleylamine (OLAM, technical grade 70%), and sodium myristate (≥99%) were bought from Sigma-Aldrich. *n*-Hexane (anhydrous), selenium (200 mesh, 99.99%), and tri-*n*-butyl-phosphine (TBP, 95%) were bought from Alfa Aesar, STREM Chemicals, and Acros Organics, respectively.

Synthesis of 4.5 ML CdSe NPLs. CdSe NPLs with a thickness of 4.5 monolayers (MLs) were prepared via an earlier reported synthesis method of Bertrand et al.[14] To obtain NPLs with a square aspect ratio, a mixture of 50/50 mol % $Cd(OAc)_2{\cdot}2H_2O/Cd(OAc)_2$ powder was added during the synthesis. Afterwards, the mixture was washed with a 1:2 mixture of MeOH/BuOH. The desired 4.5 ML NPLs were subsequently isolated via size-selective precipitation by the addition of small amounts of MeOH/BuOH and centrifugation. The 4.5 ML NPLs were finally redispersed in hexane.

Conversion of 4.5 ML CdSe NPLs in Quantum Rings. CdSe NPLs were converted into quantum rings via the previously reported procedure of Fedin et al.[10] with minor modifications. Elemental selenium was dispersed in OLAM to yield a concentration of 7.9 mg Se/mL OLAM. 1.0 milliliter of CdSe NPLs with an absorbance of 0.2 at the first exciton transition after diluting 300 times was precipitated and redispersed in 3 mL of ODE and 1.5 mL of OLAM. In the first heating step, the redispersed NPLs were heated to 80 °C for 10 min to allow the remaining hexane to evaporate. Thereafter, 200 μL of the Se-OLAM was added and heated to either 140 or 155 °C in an 8 mL reaction vial or a round-bottom flask. During the last heating step, TBP is added, followed by quick heating to 220 °C. After allowing the solution to cool down, the mixture was washed once with a 1:2 solution of MeOH/BuOH and redispersed in hexane for further characterization.

Characterization. Photoluminescence measurements were performed on an Edinburgh Instruments FLS920 spectrofluorometer meter equipped with a 450 W Xe lamp and a Hamamatsu R928 PMT detector. UV/vis absorption spectra were measured on a PerkinElmer 950 UV/VIS/NIR spectrophotometer.

TEM samples were made by drop-casting a diluted dispersion of NCs on carbon-coated TEM copper grids. Quantum rings with an edge-up orientation were prepared by the addition of a small amount of a 1:2 mixture of MeOH/BuOH to the NC dispersion and consequently drop-cast on a TEM grid. If contamination of hydrocarbons arose during imaging, the copper grid was treated

https://doi.org/10.1021/acs.chemmater.1c01618
Chem. Mater. 2021, 33, 6853−6859

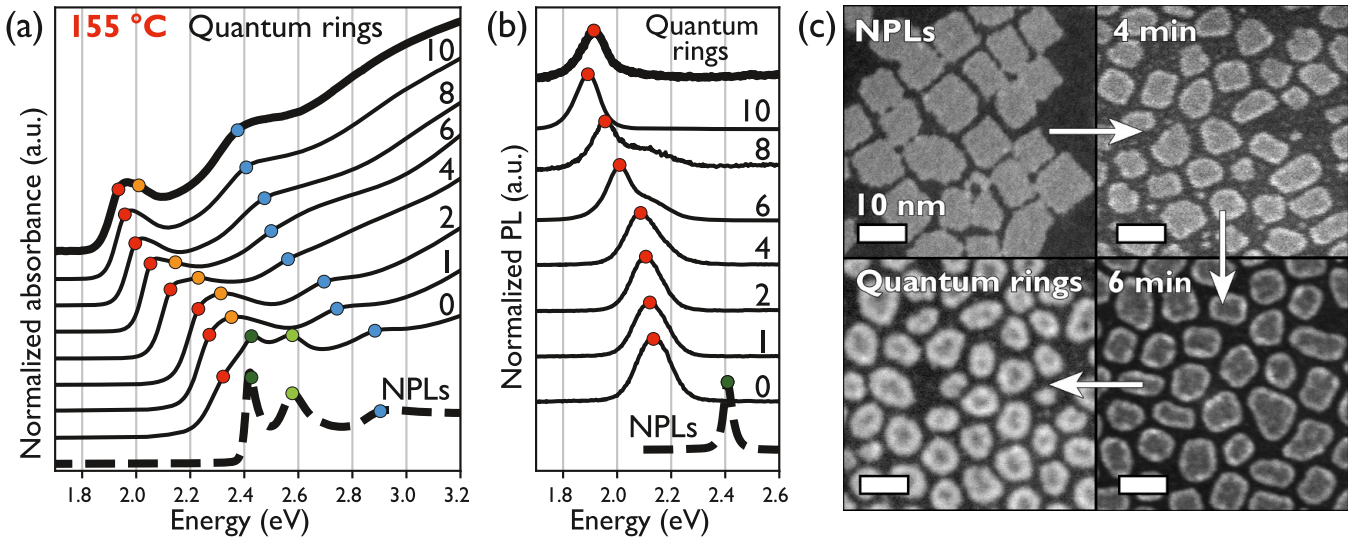

Figure 2. Monitoring the transformation of CdSe NPLs into quantum rings at 155 °C on aliquots in real time with optical spectroscopy and HAADF-STEM. (a) Absorption and (b) photoluminescence spectra of the dispersion of NPLs, aliquots taken after the mixture reached 155 °C (0 min), and after 1, 2, 4, 6, 8, and 10 min of reaction at 155 °C. For clarity, the evolving spectral features have been marked with colored circles (see the text and Figure S11). The continuous thick lines present the results for the sample that has been annealed at 220 °C following 10 min of reaction. (c) HAADF-STEM images of the original CdSe NPLs, NCs in the aliquots extracted at given times from the reaction at 155 °C, and the final quantum rings obtained after annealing at 220 °C following 10 min of reaction. All scale bars are 10 nm.

with EtOH and activated carbon according to an earlier reported procedure.[15] Low-resolution HAADF-STEM imaging was performed on either an FEI Tecnai 20FEG or Talos F200X operating at 200 keV. High-resolution HAADF-STEM imaging with atomic resolution was performed on an aberration-corrected Thermo Fisher Titan microscope operating at 300 keV.

Muffin-Tin Calculations. The energy states of the CdSe quantum rings were calculated by exploiting a three-dimensional particle in a box calculation, treating excitons as single particles. Here, realistic dimensions of a quantum ring with radius R, cylindrical radius r as $f(x, y, z) = (\sqrt{x^2 + y^2} + R^2)^2 + z^2 - r^2$, with an optional membrane with thickness $z_{membrane}$, were used. The simulations were done with a potential landscape, which can be used to solve the Schrödinger equation numerically by using the finite element method. As the exciton consists of (HH,e) and (LH,e) two-body excitations, we can mimic these as "heavy" (HH,e) or "light" (LH,e) excitonic particles using the concept of reduced mass with $m_e = 0.13$, $m_{HH} = 0.90$, and $m_{LH} = 0.19$.[16,17] From this, the reduced mass of the (HH,e) is $\mu_{e,HH} = \frac{m_e \cdot m_{HH}}{m_e + m_{HH}} = 0.11$, and (LH,e) was found to be $\mu_{e,LH} = \frac{m_e \cdot m_{LH}}{m_e + m_{LH}} = 0.077$. The calculations were performed using these two reduced masses from which the decrease in energy difference between the excitonic first states was determined. The lowest state can be visualized by taking the square magnitude of the calculated wave functions.

RESULTS AND DISCUSSION

Real-Time Characterization of the Evolution of CdSe NPLs into Rings. CdSe quantum rings are prepared by performing a thermochemical treatment with elemental selenium on 4.5 ML CdSe nanoplatelets (NPLs) following an earlier reported procedure by Fedin et al.[10] First, the CdSe NPLs are heated for several minutes in the presence of oleylamine and elemental selenium at either 140 or 155 °C. Second, in what we have assigned as the "thermal annealing" step, tri-*n*-butyl-phosphine (TBP) is added, followed by quick heating to 220 °C and cooling to room temperature. Interestingly, the end product of the treatment at 140 °C is very different from that at 155 °C. In the first case (140 °C), the NCs are still square in shape and have thickened rims at the edges and holes in the center. In the second case (155 °C), real toroidal rings are formed with rounded shapes and lateral dimensions much smaller than the original NPLs. Preparation of quantum rings at a slightly higher temperature (160 °C) resulted in the formation of spherical particles (Figure S1). We investigated the mechanism of formation by taking aliquots out of the reaction vessel during the reaction, and subsequently analyzed the intermediate reaction products with HAADF-STEM, combined with optical absorption and photoluminescence spectroscopy.

Figures 1 and S2 show the results of a typical treatment performed at 140 °C. The HAADF-STEM image of CdSe NPLs in Figure 1c shows that the NCs have lateral sizes of 14.2 × 15.7 nm^2. Moreover, the scattering intensity over a single NC is homogeneous, an indication of uniform thickness. Correspondingly, the absorption spectrum (Figure 1a) shows the characteristic features of 4.5 ML thick CdSe NPLs, i.e., the heavy-hole−electron (HH,e) and light-hole−electron (LH,e) exciton absorption peaks (dark green and light green marks, respectively), separated by 155 meV.[17,18] At a higher energy, the split-off hole−electron transition is observable (blue mark).[17,18] The photoluminescence spectrum (Figure 1b) shows a single exciton emission peak at 2.41 eV with a typical small Stokes shift of 10 meV.

The absorption spectra of aliquots taken after reaching 140 °C and after 1 and 2 min clearly show the spectrally unchanged (HH,e) and (LH,e) exciton absorption peaks. However, these spectral characteristics lose intensity and become less noticeable with time. Simultaneously, the absorption onset shifts to lower energies. Since the oscillator strength of the exciton absorption peaks is proportional to the number of CdSe unit cells present,[19] the decrease in the (HH,e) and (LH,e) absorptance peaks indicates that the surface area of the NPLs decreases during the treatment. Additionally, the shoulder appearing at lower energies between 2.2 and 2.4 eV indicates the formation of thicker regions, which corresponds

https://doi.org/10.1021/acs.chemmater.1c01618
Chem. Mater. 2021, 33, 6853−6859

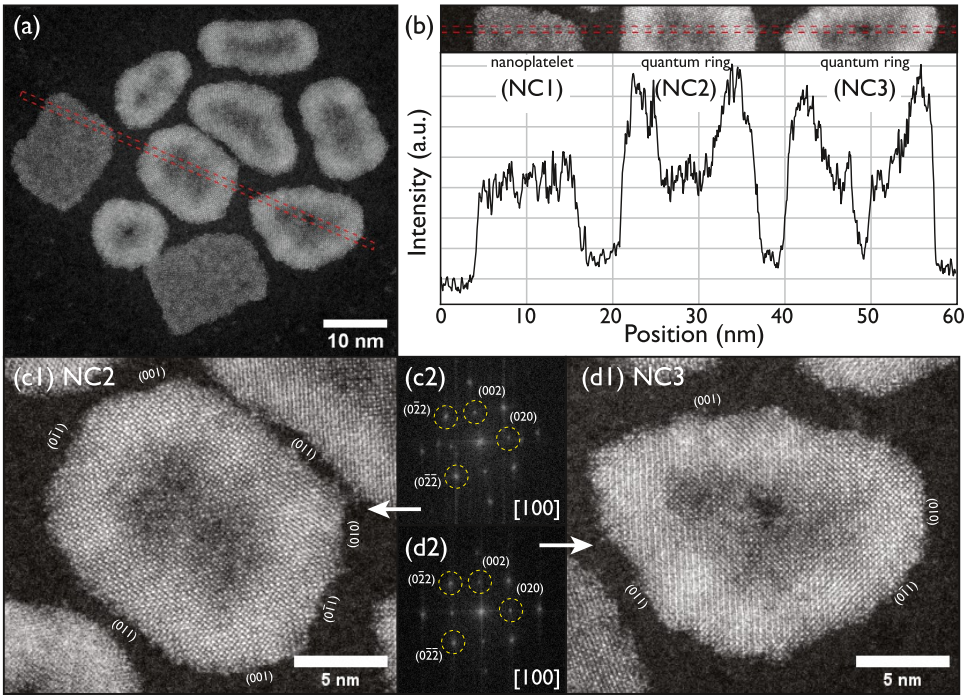

Figure 3. Detailed comparison of the crystal structure of CdSe NPLs and resulting quantum rings with HAADF-STEM after a selenium treatment at 155 °C and annealing at 220 °C. (a) HAADF-STEM image showing that the quantum rings have smaller lateral dimensions and a much thicker rim compared to the NPLs. (b) Intensity along the red dashed line in panel (a) shows different intensity profiles of an NPL and two quantum rings. The CdSe NPL (NC1) shows a relatively uniform intensity. The left quantum ring (NC2) shows a thicker rim with roughly twice the intensity of NC1 and a thinner center with a similar intensity to NC1. The right quantum ring (NC3) shows a completely formed hole in the center. Panels (c1) and (d1) show images at higher magnifications of NC2 and NC3, displaying the (almost) single-crystalline zinc blende CdSe structure, confirmed by the corresponding fast Fourier transform (FFT) patterns in panels (c2) and (d2).

to the emergence of thicker rims at the edges of the NPLs (Figures 1c and S2).

In the aliquots taken after 4 min and onwards, the contrast of the rims becomes better visible, indicating that the rims increase in relative thickness. Instead of the original absorption peaks of CdSe NPLs, two partly overlapping resonances emerge, which shift gradually to lower energy with time. The positions of the two resonances, indicated by red and orange marks, have been found by performing second-derivative analysis on the absorption spectra (Figure S4). These shifts strongly suggest that these features reflect the (HH,e) and (LH,e) exciton absorption peaks of the thickened rims. Similarly, the absorption of the (split-off hole−electron) transition (blue marks) shifts to lower energy. We observe that the Stokes shift becomes smaller and smaller as the NCs gradually obtain their final ring structure (Figure S5). A further analysis of the relation between the shape of the NC and the optical properties based on muffin-tin calculations is given below. Interestingly, in the final annealing step at 220 °C, a further reconfiguration takes place, as the NCs clearly obtain holes in the center. The increased thickness of the rims and formation of the holes were confirmed by the HAADF-STEM images, as the surface area of the NCs diminished from 200.6 ± 42.9 to 123.7 ± 20.7 nm^2 (Figure S3).

The photoluminescence spectra of the NCs feature a broad emission peak (red marks) that gradually shifts to a lower energy, reflecting emission from the (HH,e) state confined in the rim at the edges. Remarkably, the final product exhibits two emission bands: one at 2.07 and the other located at 2.18 eV. The emission peak at 2.07 eV is red-shifted with respect to the (HH,e) absorption peak at 2.11 eV, indicative of the (HH,e) transition. The optical properties of quantum rings prepared at 140 °C are further studied with photoluminescence excitation spectroscopy and varying temperatures (Section S3).

Figures 2 and S9 present the evolution of the NPLs to rings upon treating the NPLs with elemental selenium at 155 °C. The atomic reconfiguration proceeds faster and is much more pronounced than at 140 °C. The end products are quantum rings with a rounded shape, thick rims, and lateral dimensions smaller than the NPLs. It can be observed that some quantum rings still have an inner membrane of the NPLs, while other rings have a clear hole (Figure 2c). A further investigation of the atomic structure, crystallinity, and shape of the quantum rings will be presented in the next section.

The (HH,e) and (LH,e) exciton absorption features of the NPLs disappear after 2 min of reaction and are replaced by two (partial) overlapping resonances (red and orange circles) that shift strongly to lower energies with increasing reaction times (Figure 2a). It is reasonable to assume that these two resonances still indicate the (HH,e) and (LH,e) exciton absorption features but now of excitons confined to the rims that increase in thickness during the reaction. Support for this follows from muffin-tin calculations in the last section. The energy separation between the (HH,e) and (LH,e) exciton absorption features evolves from 155 meV in the NPLs to 75 meV in the quantum rings. The features marked by blue points (indicative for the (split-off hole−electron) transition) show a similar evolution to lower energies with reaction times. The photoluminescence spectrum shows one strongly broadened peak, which shifts gradually to a lower energy during ring formation (Figure 2b). In the finished quantum rings, the peak maximum is at 1.91 eV, at a considerably lower energy than for

https://doi.org/10.1021/acs.chemmater.1c01618
Chem. Mater. 2021, 33, 6853−6859

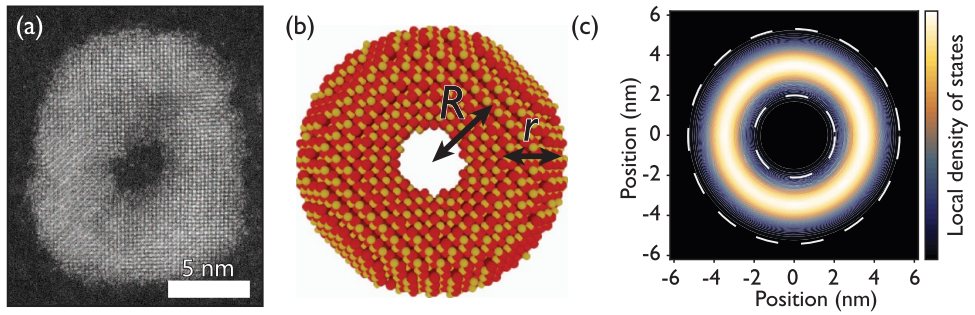

Figure 4. Muffin-tin calculations on the CdSe quantum ring system. (a) High-resolution HAADF-STEM image of a single quantum ring used as a model for the muffin-tin calculations. (b) Schematic model of a CdSe quantum ring from the top, indicating the dimensions of the quantum ring (radius *R* and cylindrical radius *r*). (c) Visualization of the squared amplitude of the lowest-energy (*s*-type) wave function, representing the heavy-hole−electron (HH,e) exciton state. The highest spatial probability is in the central part of the ring. Similar wave function maps are found for quantum rings in which the central CdSe membrane is still present (Figure S16). The muffin-tin calculations result in single-particle estimations for the energy levels of the heavy-hole and light-hole excitons, the energy difference between these resonances, and the spectral shift of these resonances in the evolution from an NPL to a ring (see the text).

the rings prepared at 140 °C. The Stokes shift between the broad (HH,e) luminescence and absorption peak is larger than for the NPLs (Figure S12).

Shape and Crystal Structure of the Rings Formed at 155 °C. We have performed a detailed atomically resolved characterization of the final CdSe rings using aberration-corrected HAADF-STEM imaging (see Figures 3 and S13). To compare the shape of NPLs and quantum rings prepared at 155 °C, we intentionally mixed pure solutions of both NCs.

Several aspects can be observed. First, the average surface area of the quantum rings (132.4 ± 35.8 nm^2) is smaller than that of the original NPLs (233.1 ± 45.5 nm^2) (see also Figure S10). Second, as the intensity in HAADF-STEM imaging scales with the atomic number *Z* (so-called *Z*-contrast imaging), we can use the intensity to identify if a hole is formed in the center of the rings. We stress that HAADF-STEM is a powerful tool to investigate the holes of quantum rings, as these are hardly visible with conventional bright-field TEM (Figure S14). We took a line profile across the NCs (Figure 3b) and used the intensity of the carbon support as a reference. If the intensity of the thinnest part of an NC is higher than the carbon support, it indicates that there is a membrane left inside the NC. We find that many quantum rings still have a membrane inside with the thickness of the original NPLs, i.e., 1.3 nm.[20] This is clearly observable from Figure 3b, which shows an intensity line profile along the red dashed line in Figure 3a. The measured area is shown in the inset on top of Figure 3b, so that the locations of the three measured NCs are aligned with the line profile below. The leftmost NC (NC1) with a relatively uniform intensity is a CdSe NPL. The NC in the middle (NC2) is a typical example of a quantum ring with the 1.3 nm thick membrane still present. The intensity in the center of NC2 is similar to that of the NPL on its left, and the intensity in the rim of NC2 amounts to roughly twice the intensity of NC1. In Figure 3c1, an image of NC2 at higher magnification is shown, in which a continuous crystal lattice can be observed. In contrast, the rightmost NC (NC3) shows a much lower intensity in the center, which is similar to the carbon support, thus showing that a hole has been formed. A HAADF-STEM image of NC3 at higher magnification is shown in Figure 3d1, confirming the small hole (region with no atoms) in the center of the NC.

The results shown here do not agree with the formation mechanism that has been put forward by Fedin et al., featuring Se-induced etching of the top and bottom surfaces. First, the reduced lateral dimensions and the formation of thicker rims show that the atomic reconfiguration predominantly occurs at the edges. Second, the frequent observation of membranes with a thickness similar to that of the original NPLs in the center of the quantum rings indicates that etching of the top and bottom surfaces does not occur. Instead, our results show that CdSe units from the vertical edge planes are redeposited on the top and bottom surfaces at the rim, resulting in a pronounced thickening of the rim. In that scenario, the top and bottom planes terminated by both acetate and oleate remain intact. The exact moment at which a hole is formed, and why, is not entirely understood. Nevertheless, we observe that hole formation is more pronounced after the thermal annealing step at 220 °C. Inhomogeneous crystalline stress[21] can be a reason for the formation of hole in the center of the NC, resulting in a genuine ring.

Representative high-resolution images of quantum rings (Figure 3c1,d1) show single-crystal zinc blende CdSe structures oriented on the [100] zone axis, confirmed by the corresponding fast Fourier transform (FFT) patterns depicted in Figure 3c2,d2. These observations are consistent with the analysis of several other quantum rings.

Although most quantum rings lack defects such as grain boundaries or dislocations, slight misorientations are present in small areas. For instance, at the left-bottom corner of the quantum ring in Figure 3d1, a slight difference in orientation of atomic columns is present compared to the rest of the crystal, which we attribute to bending after release of strain. Next to the areas with rounded edges, four specific facets are favored, namely, (001), (010), (011), and (01−1) facets, as indicated in Figure 3c1,d1.

Figure S15 shows HAADF-STEM images of quantum rings, which are oriented edge-up. The thickness of the quantum rings varies between 2.5 and 3.5 nm, although domains up to 5.0 nm are observed as well. This corresponds to an average thickness of 9−12 monolayers of CdSe and shows that the rings can become 2−3 times thicker than the 1.3 nm thick 4.5 ML NPLs,[20] which is in line with the image intensity profile in Figure 3b. Furthermore, the thicker corners and rounded shapes of the rings suggest that the atomic reconfiguration occurs most severely at the corners of the NPLs. The atomistic mechanism and role of selenium in this atomic reconfiguration cannot be deduced from our results and will require advanced

https://doi.org/10.1021/acs.chemmater.1c01618
Chem. Mater. 2021, 33, 6853−6859

molecular dynamics modeling. Thus, in the reshaping of an NPL into a ring, the large top and bottom surfaces remain highly stable. This is in contrast to the edges and corners that undergo a remarkable atomic reconfiguration. The formation of holes in the rings occurs mainly in the last "annealing step" at 220 °C, something that is clearly visible in the preparation of the rings at 140 °C.

Relation between the Spectral Features and the Shape of the CdSe Quantum Rings. To relate the absorption and emission features of the CdSe quantum rings prepared at 155 °C to their shape and dimensions, we have performed simple muffin-tin model calculations using a model quantum ring with dimensions similar to the prepared quantum rings. The results are quantitatively compared with model calculations on a rectangular 4.5 ML thick CdSe NPL ($1.3 \times 10 \times 10$ nm^3). A model of the quantum ring is shown in Figure 4b. The prepared quantum rings are relatively polydisperse and were approximated as toroidal NCs with a radius R of 3.6 nm and a cylindrical radius r of 1.6 nm, as a decent averaged model.

We consider the exciton states as electron−hole-composed single particles with a reduced effective mass, which is derived from the conduction band and heavy-hole (HH) and light-hole (LH) valence bands. We solve the Schrödinger equation for a particle with this effective mass confined in the CdSe ring of Figure 4a, thus neglecting the electron−hole Coulomb attraction. Figure 4c presents the lowest (HH,e) state in the ring, with an s-like envelope function, although with a genus of 1. The single-particle wave functions are delocalized over the entire quantum ring, even if we take a model with a membrane inside the ring with the thickness of a CdSe NPL (see Figure S16). In the latter case, the energy of the states is nearly equal to those for the modeled quantum ring without the membrane. For the (HH,e) exciton state, we use a reduced effective mass $\mu_{HH,e}$ of 0.11 in agreement with literature values.[16,17] For the (LH,e) exciton state, we use a reduced mass $\mu_{LH,e}$ of 0.09, instead of the literature value of 0.077[16,17] to obtain a better quantitative agreement with the spectral results.

First, we examine the 4.5 ML CdSe NPLs. The experimentally determined energy difference between the (HH,e) and (LH,e) peaks is 155 meV. Using the slightly adapted reduced mass for the (LH,e) exciton, we calculate a difference of 152 meV (Figure S16), in good agreement with the experimental result. Next, we examined the formed quantum rings. The energy difference between the (HH,e) and (LH,e) peaks in the quantum rings is smaller due to the reduced quantum confinement in the quantum ring versus the NPL. Since the (HH,e) and (LH,e) peaks overlap, we used second-derivative analysis to decompose the absorption spectrum and found an energy difference of 75 meV (Figure S11). The muffin-tin calculation resulted in an energy difference of 105 meV, in reasonable agreement with the experimental result.

The calculations provide a single-particle result, neglecting the electron−hole attraction energy. However, if we assume that the electron−hole attraction for the (HH,e) and (LH,e) states is similar to a good degree, our single-particle calculation is reasonable. We thus confirm that the red-shifted peaks (red and orange marks) in the absorption spectrum of the quantum rings (Figure 2a) are due to the (HH,e) and (LH,e) states similar to the two sharp peaks in an NPL.

In analogy, we assign the broad emission of the quantum rings to the (HH,e) exciton state. The considerably broader peak of emission reflects inhomogeneous broadening as the shapes and sizes of the quantum rings are not entirely monodisperse (see Figures 2 and S15), in contrast to the uniform thickness of the NPLs. Now, we consider the strong red shift of the (HH,e) exciton state in the absorption spectrum of the quantum rings with respect to the NPLs. Experimentally, this red shift is 492 meV, while our muffin-tin calculation provides an energy shift of 407 meV. We remark that a slightly larger quantum ring (cylinder radius r of 1.9 instead of 1.6 nm) provides a red shift increasing to 567 meV, indicating that the cylinder radius is a critical factor in the red shift. In the evolution from platelets to rings, both the reduced (HH,e)−(LH,e) energy separation and the absolute red shift of these resonances can be explained in a consistent manner by the presented model.

CONCLUSIONS

By combining HAADF-STEM imaging with absorption and photoluminescence spectroscopy, we were able to follow the evolution of CdSe nanoplatelets to CdSe quantum rings. Our results show that atomic reconfigurations at the edges result in intermediate crystal shapes with thickened rims, while the formation of a hole inside these nanocrystals occurs only at the end of the process at elevated temperatures. High-resolution HAADF-STEM images show how the cubic zinc blende crystal structure and facet termination can be in compliance with the ring shape. The quantum rings still display the (HH,e) and (LH,e) exciton resonances, albeit less separated in energy due to the reduced confinement. As CdSe rings are the first crystals in a topological class with genus 1, they might be of interest for fundamental studies of the optoelectronic properties in a magnetic field and perhaps form the basis for optical quantum sensors.

ASSOCIATED CONTENT

Supporting Information

The Supporting Information is available free of charge at https://pubs.acs.org/doi/10.1021/acs.chemmater.1c01618.

Additional HAADF-STEM images of quantum rings prepared at 140, 155, and 160 °C; comparison of HAADF-STEM versus bright-field TEM imaging; calculated surface area of aliquots and final quantum rings from HAADF-STEM images; second-derivative analysis and calculated Stokes shifts of quantum rings prepared at 140 and 155 °C; photoluminescence excitation spectra and temperature-dependent spectroscopy of quantum rings prepared at 140 °C; high-resolution HAADF-STEM imaging of aliquots and quantum rings with edge-up orientation; and additional wave function maps of muffin-tin calculations (PDF)

AUTHOR INFORMATION

Corresponding Author

Daniel Vanmaekelbergh − *Condensed Matter & Interfaces, Debye Institute for Nanomaterials Science, Utrecht University, 3508TA Utrecht, The Netherlands;* orcid.org/0000-0002-3535-8366; Email: d.vanmaekelbergh@uu.nl

Authors

Bastiaan B. V. Salzmann − *Condensed Matter & Interfaces, Debye Institute for Nanomaterials Science, Utrecht*

University, 3508TA Utrecht, The Netherlands; orcid.org/0000-0002-8055-4681

Jara F. Vliem − *Condensed Matter & Interfaces, Debye Institute for Nanomaterials Science, Utrecht University, 3508TA Utrecht, The Netherlands*

D. Nicolette Maaskant − *Condensed Matter & Interfaces, Debye Institute for Nanomaterials Science, Utrecht University, 3508TA Utrecht, The Netherlands;* orcid.org/0000-0001-5979-4296

L. Christiaan Post − *Condensed Matter & Interfaces, Debye Institute for Nanomaterials Science, Utrecht University, 3508TA Utrecht, The Netherlands;* orcid.org/0000-0001-9271-7225

Chen Li − *EMAT and Nanolab Centre of Excellence, Antwerp University, 2020 Antwerp, Belgium*

Sara Bals − *EMAT and Nanolab Centre of Excellence, Antwerp University, 2020 Antwerp, Belgium;* orcid.org/0000-0002-4249-8017

Complete contact information is available at: https://pubs.acs.org/10.1021/acs.chemmater.1c01618

Author Contributions

The manuscript was written through contributions of all authors. All authors have given approval for the final version of the manuscript.

Notes

The authors declare no competing financial interest.

■ ACKNOWLEDGMENTS

Hans Meeldijk is kindly acknowledged for helping with electron microscopy at Utrecht University. B.B.V.S. and D.V. acknowledge the Dutch NWO for financial support via the TOP-ECHO grant no. 715.016.002. D.V. acknowledges financial support from the European ERC Council, ERC Advanced grant 692691 "First Step". D.V. and L.C.P. acknowledge the Dutch NWO for financial support via the TOP-ECHO grant nr. 718.015.002. S.B acknowledges financial support from the European ERC Council, ERC Consolidator grant 815128. This project has received funding from the European Union's Horizon 2020 research and innovation program under grant agreement no. 731019 (EUSMI).

■ REFERENCES

(1) Murray, C. B.; Norris, D. J.; Bawendi, M. G. Synthesis and characterization of nearly monodisperse CdE (E = sulfur, selenium, tellurium) semiconductor nanocrystallites. *J. Am. Chem. Soc.* **1993**, *115*, 8706−8715.

(2) Peng, X.; Manna, L.; Yang, W.; Wickham, J.; Scher, E.; Kadavanich, A.; Alivisatos, A. P. Shape control of CdSe nanocrystals. *Nature* **2000**, *404*, 59−61.

(3) Ithurria, S.; Dubertret, B. Quasi 2D colloidal CdSe platelets with thicknesses controlled at the atomic level. *J. Am. Chem. Soc.* **2008**, *130*, 16504−16505.

(4) Cho, K. S.; Talapin, D. V.; Gaschler, W.; Murray, C. B. Designing PbSe nanowires and nanorings through oriented attachment of nanoparticles. *J. Am. Chem. Soc.* **2005**, *127*, 7140−7.

(5) Xiong, X.; Zhou, T.; Liu, X.; Ding, S.; Hu, J. Surfactant-mediated synthesis of single-crystalline Bi3O4Br nanorings with enhanced photocatalytic activity. *J. Mater. Chem. A* **2017**, *5*, 15706−15713.

(6) Klein, E.; Heymann, L.; Hungria, A. B.; Lesyuk, R.; Klinke, C. Colloidal lead iodide nanorings. *Nanoscale* **2018**, *10*, 21197−21208.

(7) Kull, S.; Heymann, L.; Hungria, A. B.; Klinke, C. Synthesis of Single-Crystalline Lead Sulfide Nanoframes and Nanorings. *Chem. Mater.* **2019**, *31*, 5646−5654.

(8) Hartmann, N. F.; Otten, M.; Fedin, I.; Talapin, D.; Cygorek, M.; Hawrylak, P.; Korkusinski, M.; Gray, S.; Hartschuh, A.; Ma, X. Uniaxial transition dipole moments in semiconductor quantum rings caused by broken rotational symmetry. *Nat. Commun.* **2019**, *10*, No. 3253.

(9) Xiao, J.; Liu, Y.; Steinmetz, V.; Caglar, M.; Mc Hugh, J.; Baikie, T.; Gauriot, N.; Nguyen, M.; Ruggeri, E.; Andaji-Garmaroudi, Z.; et al. Optical and Electronic Properties of Colloidal CdSe Quantum Rings. *ACS Nano* **2020**, *14*, 14740−14760.

(10) Fedin, I.; Talapin, D. V. Colloidal CdSe Quantum Rings. *J. Am. Chem. Soc.* **2016**, *138*, 9771−4.

(11) Kleemans, N. A. J. M.; Blokland, J. H.; Taboada, A. G.; van Genuchten, H. C. M.; Bozkurt, M.; Fomin, V. M.; Gladilin, V. N.; Granados, D.; García, J. M.; Christianen, P. C. M.; et al. Excitonic behavior in self-assembled InAs/GaAs quantum rings in high magnetic fields. *Phys. Rev. B: Condens. Matter Mater. Phys.* **2009**, *80*, No. 155318.

(12) Sellers, I. R.; Whiteside, V. R.; Govorov, A. O.; Fan, W. C.; Chou, W. C.; Khan, I.; Petrou, A.; McCombe, B. D. Coherent Aharonov-Bohm oscillations in type-II (Zn,Mn)Te/ZnSe quantum dots. *Phys. Rev. B: Condens. Matter Mater. Phys.* **2008**, *77*, No. 885.

(13) Kagan, C. R.; Bassett, L. C.; Murray, C. B.; Thompson, S. M. Colloidal Quantum Dots as Platforms for Quantum Information Science. *Chem. Rev.* **2021**, *121*, 3186−3233.

(14) Bertrand, G. H.; Polovitsyn, A.; Christodoulou, S.; Khan, A. H.; Moreels, I. Shape control of zincblende CdSe nanoplatelets. *Chem. Commun.* **2016**, *52*, 11975−11978.

(15) Li, C.; Tardajos, A. P.; Wang, D.; Choukroun, D.; Van Daele, K.; Breugelmans, T.; Bals, S. A simple method to clean ligand contamination on TEM grids. *Ultramicroscopy* **2021**, *221*, No. 113195.

(16) Kim, Y. D.; Klein, M. V.; Ren, S. F.; Chang, Y. C.; Luo, H.; Samarth, N.; Furdyna, J. K. Optical properties of zinc-blende CdSe and ZnxCd1-xSe films grown on GaAs. *Phys. Rev. B: Condens. Matter* **1994**, *49*, 7262−7270.

(17) Ithurria, S.; Tessier, M. D.; Mahler, B.; Lobo, R. P.; Dubertret, B.; Efros, A. L. Colloidal nanoplatelets with two-dimensional electronic structure. *Nat. Mater.* **2011**, *10*, 936−941.

(18) Christodoulou, S.; Climente, J. I.; Planelles, J.; Brescia, R.; Prato, M.; Martin-Garcia, B.; Khan, A. H.; Moreels, I. Chloride-Induced Thickness Control in CdSe Nanoplatelets. *Nano Lett.* **2018**, *18*, 6248−6254.

(19) Elliott, R. J. Intensity of Optical Absorption by Excitons. *Phys. Rev.* **1957**, *108*, 1384−1389.

(20) Achtstein, A. W.; Antanovich, A.; Prudnikau, A.; Scott, R.; Woggon, U.; Artemyev, M. Linear Absorption in CdSe Nanoplates: Thickness and Lateral Size Dependency of the Intrinsic Absorption. *J. Phys. Chem. C* **2015**, *119*, 20156−20161.

(21) Dufour, M.; Qu, J.; Greboval, C.; Methivier, C.; Lhuillier, E.; Ithurria, S. Halide Ligands To Release Strain in Cadmium Chalcogenide Nanoplatelets and Achieve High Brightness. *ACS Nano* **2019**, *13*, 5326−5334.